Available online at www.sciencedirect.com
ScienceDirect
Geochimica et Cosmochimica Acta 73 (2009) 4907–4917
Geochimica et Cosmochimica Acta
www.elsevier.com/locate/gca

Hydrothermal jarosite and hematite in a pyroxene-hosted melt inclusion in martian meteorite Miller Range (MIL) 03346: Implications for magmatic-hydrothermal fluids on Mars

Francis M. McCubbin [a,*], Nicholas J. Tosca [b], Alexander Smirnov [c,1], Hanna Nekvasil [a], Andrew Steele [c], Marc Fries [c,2], Donald H. Lindsley [a]

[a] Department of Geosciences, Stony Brook University, Stony Brook, NY 11794-2100, USA
[b] Department of Organismic and Evolutionary Biology, Harvard University, 26 Oxford St., Cambridge, MA 02138, USA
[c] Geophysical Laboratory, Carnegie Institution of Washington, 5251 Broad Branch Rd., N.W, Washington, DC 20015, USA

Received 3 February 2009; accepted in revised form 5 May 2009; available online 12 May 2009

Abstract

Low-temperature aqueous processes have been implicated in the generation of jarosite and hematite on the martian surface, but little is known regarding the role that high-temperature magmatic fluids may have played in producing similar assemblages on Mars. We have identified jarosite and hematite in a clinopyroxene-hosted melt inclusion in martian meteorite MIL 03346 that shows evidence of having been hydrothermally precipitated. In addition to jarosite and hematite, the melt inclusion contains titanomagnetite, pyrrhotite, potassic-chlorohastingsite, an iron-rich silicate glass and possibly goethite. These phases were identified and characterized using scanning electron microscopy (SEM), con-focal Raman-spectroscopy and electron probe microanalysis (EPMA).

Based on observed textural relationships and the compositions of the hosted phases, we report that the jarosite-bearing melt inclusion in MIL 03346 has recorded a fluid-rich history that began in the magmatic stage and continued to low-temperatures. This history begins at entrapment of a volatile-rich silicate melt that likely reached fluid-saturation after only minor crystallization within the melt inclusion. This fluid, rich in chlorine, reacted with surrounding silicate material to produce the potassic-chlorohastingsite. As cooling proceeded, the liquid phase eventually became more oxidized and reacted with the pyrrhotite. Sulfide oxidation resulted in SO_4^{2-} formation and concomitant acid production, setting the stage for jarosite formation once the fluid cooled beyond the upper thermal stability of jarosite (~200 °C). As the fluid cooled below 200 °C, jarosite continued to precipitate with hematite and/or goethite until equilibrium was established or reactions became kinetically unfavorable.

This work suggests an additional jarosite–hematite formation pathway on Mars; one that may be important wherever magmatic-hydrothermal fluids come into contact with primary sulfide grains at the martian surface or subsurface. Moreover, hydrothermal fluids rich in chlorine, sulfur, and iron are important for ore-forming processes on Earth, and their indirect identification on Mars may have important implications for ore-formation on Mars.

1. INTRODUCTION

Identification of alteration assemblages in martian surface rocks containing jarosite and hematite have led to a variety of studies focused on constraining both the formation mechanism and the chemical nature of the waters involved in the precipitation of these assemblages (e.g.,

* Corresponding author. Present address: Geophysical Laboratory, Carnegie Institute of Washington, 5251 Broad Branch Rd., Washington, N.W, DC 20015, USA.
E-mail address: fmccubbin@ciw.edu (F.M. McCubbin).
[1] Present address: Department of Geosciences, Stony Brook University, Stony Brook, NY11794-2100, USA.
[2] Present address: Jet Propulsion Laboratory, M/S 183-301, 4800 Oak Grove Drive, Pasadena, CA 91109, USA.

0016-7037/$ - see front matter © 2009 Elsevier Ltd. All rights reserved.
doi:10.1016/j.gca.2009.05.031

Glotch et al., 2004; Madden et al., 2004; King and McSween, 2005; McLennan et al., 2005; Navrotsky et al., 2005; Tosca et al., 2005; Papike et al., 2006; Glotch and Rogers, 2007; Hurowitz and McLennan, 2007; Tosca et al., 2008a). Such constraints have wide-ranging implications for understanding the history of the planet, from the timing of a functioning hydrologic cycle to the origin and sustainability of life on Mars. Thus far, much of our understanding of the formation mechanisms behind jarosite–hematite assemblages on Mars is through low-temperature diagenetic processes; however, little is known regarding the role that high-temperature magmatic fluids may have played in producing these assemblages on Mars.

The formation of jarosite–hematite assemblages requires the presence of a highly acidic (pH < 4), oxidized S- and Fe-rich brine (e.g., Papike et al., 2006). Magmatic fluids capable of producing such assemblages must also have these characteristics at low-temperatures. Identification of such fluids capable of producing jarosite and hematite upon cooling in martian samples is problematic and can only be done indirectly by studying martian meteorites that show subsolidus assemblages in melt pockets isolated from potentially infiltrating meteoric waters. Such isolated melt pockets may be best represented by mineral-hosted melt inclusions. The observation of a Cl-rich amphibole (Sautter et al., 2006) in the martian meteorite Miller Range 03346 (MIL 03346) represents a major step in the search for melt inclusions that have hosted concentrated fluids that produced subsolidus assemblages. Cl-amphibole is a non-magmatic hydrothermal amphibole (Vanko, 1986; McCormick and McDonald, 1999; Mazdab, 2003), indicating the presence and retention of a concentrated hydrothermal fluid or saline melt into the subsolidus thermal regime. This work reports on further investigation of melt inclusions in MIL 03346 with a focus on identification and interpretation of subsolidus mineral assemblages and the nature of the fluids from which they formed.

MIL 03346 is a member of the nakhlite class of SNC (martian) meteorites. It is a cumulate clinopyroxenite with cumulus clinopyroxene and olivine grains (Dyar et al., 2005; Day et al., 2006; Imae and Ikeda, 2007). Interstitial to these cumulus grains are skeletal titanomagnetites, fayalitic olivines, chromite, pyrrhotite, cristobalite, apatite, chalcopyrite, and glass (Dyar et al., 2005; Aoudjehane et al., 2006; Day et al., 2006; Sautter et al., 2006; Imae and Ikeda, 2007). Some of the cumulus pyroxenes and olivines contain large ($\sim$50–100 μm) polyphase melt inclusions. These partially crystallized melt inclusions are reported to contain titanomagnetite, fayalitic olivine, chromite, pyrrhotite, cristobalite, apatite, chalcopyrite, glass, and Cl-rich amphibole (Dyar et al., 2005; Aoudjehane et al., 2006; Day et al., 2006; Sautter et al., 2006; Imae and Ikeda, 2007). MIL 03346 also has a low-temperature vein alteration assemblage reported to include Cl-poor smectite, iddingsite and jarosite (Herd, 2006; Sautter et al., 2006; Vicenzi et al., 2007a).

While MIL 03346 is broadly representative of the nakhlites, in detail, it is unique in several ways. First, it is a highly oxidized rock; in fact, it has been referred to as the most oxidized martian meteorite found to date (Dyar et al., 2005) with the mesostasis indicating an oxygen fugacity close to the QFM buffer (Dyar et al., 2005; Righter et al., 2008). This is thought to be the result of an oxidizing magmatic environment, not a product of martian or terrestrial weathering (Dyar et al., 2005; Righter et al., 2008). Yet, the oxidation event appears to have occurred in the late magmatic stage since the cumulus pyroxene cores from MIL 03346 exhibit low ferric iron (Domeneghetti et al., 2006, 2007), which indicates that the high ferric iron contents are concentrated in cumulus pyroxene rims and mesostasis. Aside from its oxidation state, MIL 03346 is currently the only nakhlite known to contain Cl-rich amphibole within some of its mineral-hosted melt inclusions. Lastly, MIL 03346 is the only martian meteorite to date reported to contain jarosite among its alteration phases, albeit only in the post-crystallization vein assemblage (Herd, 2006; Vicenzi et al., 2007a,b). Collectively, these observations are central to placing constraints on the nature of fluids involved in the petrogenesis of MIL 03346.

Although the hydrothermal nature of Cl-rich amphibole found in MIL 03346 has not been questioned, the source of the Cl in the fluids is less clear. Sautter et al. (2006) suggested that the high chlorinity and oxidation state arose from magma assimilation of Cl- and ferric Fe-rich soils at or near the martian surface. However, this hypothesis is inconsistent with the low ferric iron contents of the cumulus clinopyroxene cores where the melt inclusions are found, and no mechanism has yet been proposed that would introduce such contaminated magma into melt inclusions after the formation of their pyroxene hosts.

Sautter et al. (2006) ruled out magmatic-hydrothermal fluids from uncontaminated magma as a source of the Cl-amphibole based on the observed low-temperature alteration vein assemblages (which were consistent with formation via water-rich, chlorine-poor fluid/rock interactions). However, there is no evidence that the Cl-amphibole and the low-temperature vein assemblages must have formed from the same fluid, since vein-hosted low-temperature assemblages can be produced by meteoric waters at a variety of post-magmatic stages. For example, apatite from the Chassigny meteorite records high-temperature (> 700 °C) Cl-rich fluid–rock interaction (McCubbin and Nekvasil, 2008); however, low-temperature [$\leqslant$150 °C (Bridges et al., 2001)] alteration products within the meteorite record the presence of a fluid that did not contain high Cl. Given the potential importance of magmatic fluids in assessing the geologic history of martian magmatic systems, it is vital to search for subsolidus assemblages that could constrain the nature of such fluids.

The development of a magmatic fluid-mediated subsolidus assemblage requires an environment in which fluids are retained long enough for precipitation to occur. In rocks with fine-grained mesostasis, magmatic fluid retention into the subsolidus thermal regime may only have been possible in melt inclusions. Therefore, we investigated melt inclusions in MIL 03346 for subsolidus mineral assemblages. However, because melt inclusion rupture does occur, we focused only on those inclusions that appear to have

remained sealed over a significant period of their thermal history.

2. ANALYTICAL TECHNIQUES

2.1. Image acquisition

Back-scattered electron (BSE) imaging and energy-dispersive spectroscopy (EDS) were performed at the Geophysical Laboratory, (Washington, DC) on a JEOL JSM 6500F scanning electron microscope with a field emission gun equipped with a liquid N_2-cooled sapphire Si(Li) EDS detector (EDAX) using a 15 kV operating voltage.

2.2. Raman spectroscopy

Raman micro-spectroscopy was performed at the Geophysical Laboratory, (Washington, DC) using a WITec-SNOM AFM instrument customized to accommodate confocal imaging geometry. A frequency-doubled solid-state YAG laser operating at 0–50 mW output power was used as the excitation source. The resolvable spot size for this technique is approximately 360 nm^2. A detailed description of this technique has been published previously by Steele et al. (2007).

2.3. EPMA Analysis

Electron probe microanalysis (EPMA) of Cl-amphibole from a thin section (MIL 03346, 114 provided by NASA JSC) was performed at Stony Brook University (Stony Brook, NY) using a Cameca Camebax electron microprobe. An accelerating voltage of 15 kV and a nominal beam current of 10 nA were used during all analyses. A beam diameter of 3–10 μm was used for all analyses of Cl-rich amphibole. All other phases were analyzed on a JEOL JXA-8800L microprobe at the Geophysical Laboratory (Washington, DC). An accelerating voltage of 15 kV and a nominal beam current of 10 nA were used for all analyses with a beam diameter ranging from ~2 to 10 μm.

3. RESULTS/DATA REDUCTION

3.1. Petrographic observations

Determining which melt inclusions have been breached and which ones have not is an important criterion for petrogenetic interpretation. For MIL 03346, melt inclusions that remained sealed at least into the high-temperature hydrothermal regime can be distinguished by the presence of Cl-amphibole. Because this amphibole requires a fluid or saline melt, it would only be present within areas of the meteorite where such a phase had remained trapped. It is recognized, however, that its absence does not fully imply rupture because each melt inclusion represents only a two-dimensional slice through a three-dimensional system. Melt inclusions that have clearly ruptured have a texture and mineralogy identical to the mesostasis (Fig. 1a–d). The mesostasis phases fayalitic olivine and silica are absent from the Cl-amphibole-bearing melt inclusions investigated, therefore the presence of these mesostasis phases in a melt inclusion likely indicates melt inclusion rupture. On this basis, more than half of the melt inclusions observed appeared to have ruptured. Olivine-hosted melt inclusions, which do not rupture as easily as pyroxene-hosted melt inclusions due to lack of cleavage (Veksler, 2006), were not observed in the thin-section we analyzed.

Petrographic descriptions of the mineral assemblages of MIL 03346 have been reported by Treiman (2005), Dyar et al. (2005), Day et al. (2006), Sautter et al. (2006), Imae and Ikeda (2007) and a number of abstracts. Our study of the cumulus and mesostasis mineral phases has yielded observations broadly consistent with previous studies, with one important new finding – the presence of jarosite, finely intergrown with hematite ± minor goethite in a clinopyroxene-hosted melt inclusion. This assemblage was conclusively identified by Raman micro-spectroscopy (Figs. 2a and b, and 3) in a 10–15 μm^2 area surrounding a magmatic pyrrhotite grain within a Cl-rich amphibole-bearing melt inclusion. Other phases within this melt inclusion include titanomagnetite and two intergrown amorphous Fe–Si-rich phases (referred to herein as Fe–Si-rich glass) containing submicron phosphate. Of these phases, Cl-amphibole, jarosite, and hematite (±goethite) typically form in the subsolidus thermal regime (Stoffregen, 1993; Mazdab, 2003) and likely require the presence of an aqueous phase or saline melt.

3.2. Crystal chemistry of the Cl-rich amphibole

EPMA analyses of two Cl-rich amphiboles are shown in Table 1. The crystal-chemical formulae of the amphibole analyses were calculated based on 24 anions, 15 cations and 13 cations in order to assess the reliability of calculated values for ferric iron (Table 2). Recalculating the normalization scheme on the basis of 15 cations was found to be the most accurate formulaic representation because the 24-anion normalization resulted in significant over population of the A-site, and the 13-cation normalization required atypical tetrahedral-site substitutions (i.e., $Si + Al < 8$ atoms).

The resulting amphibole stoichiometry (ideally: $A_{0-1}M4_2M(1-3)_5[T_8O_{22}]O3_2$) is presented at the bottom of Table 2. Because chlorine did not completely fill the amphibole O(3) site, we assumed that the remaining space was occupied by OH^- (the presence of OH^- in the amphibole was verified by Raman spectroscopy). If instead, some of the remaining space is filled by O^{2-}, our calculated ferric iron content would increase until an electroneutral formula was attained. From our normalization scheme, we calculated $Fe^{3+}/\sum Fe$ values ranging from 0.09 to 0.14, which is significantly less ferric iron than calculated by previous investigators. Although the ferric iron contents were not directly measured, it must be noted that the high ferric iron contents implied by the stoichiometric computations conducted by previous investigators can arise from their use of a normalization scheme based on 13 cations (Sautter et al., 2006) and not necessarily reflect the actual ferric/ferrous ratio of the mineral (see Table 2 for an example of this). The chlorine contents of this amphibole are very high

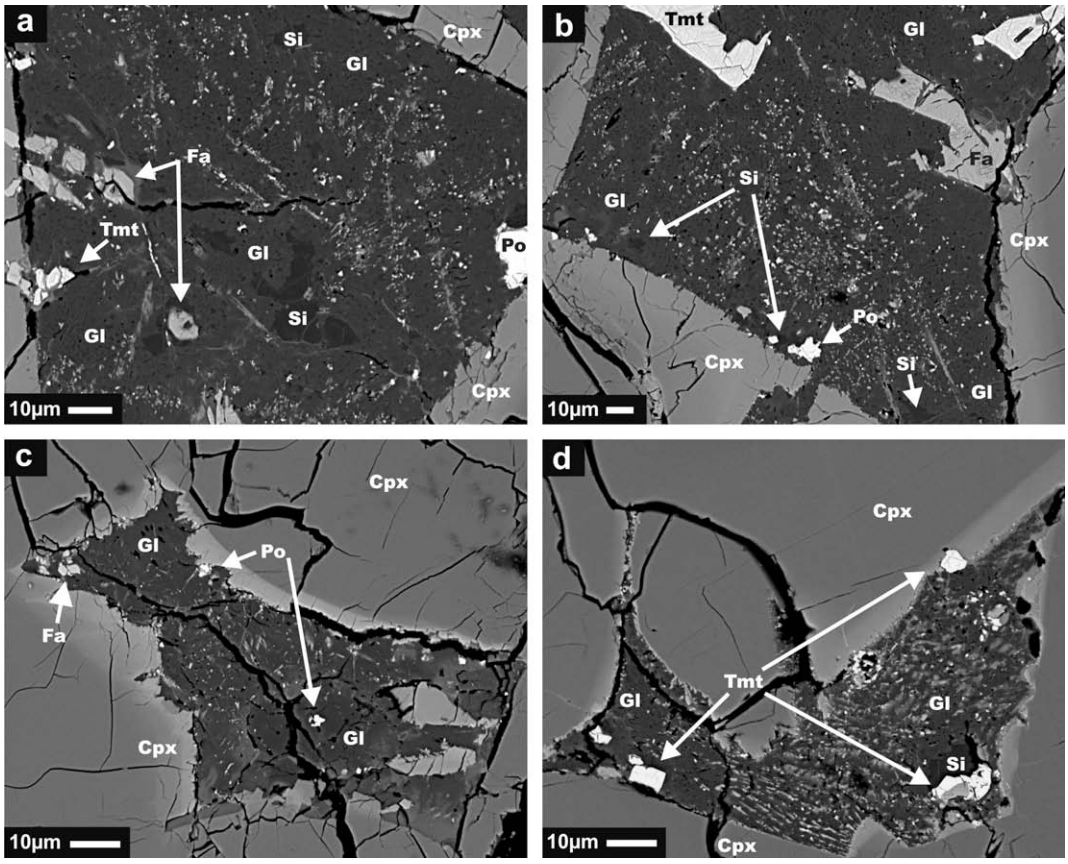

Fig. 1. Back-scattered electron images of mesostasis and breached melt inclusions from MIL 03346. Identified phases are labeled, and the phase abbreviations are indicated as follows: Tmt, titanomagnetite; Po, pyrrhotite; Gl, glass/maskelynite; Fa, fayalitic olivine; Si, silica phase; Cpx, cumulus clinopyroxene. (a) Mesostasis (b) mesostasis (c) breached melt inclusion (d) breached melt inclusion.

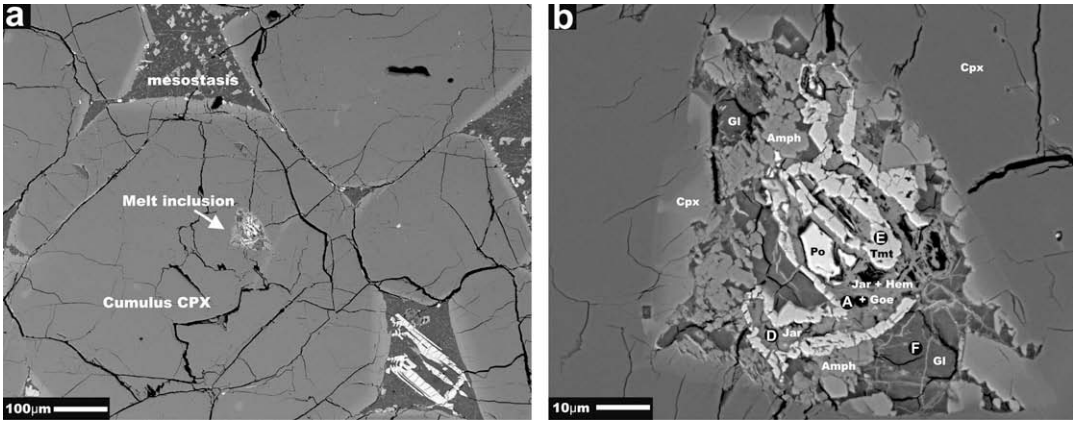

Fig. 2. Back-scattered electron images of the jarosite-bearing melt inclusion (a) low-magnification image showing the cumulus clinopyroxene host and surrounding mesostasis. (b) High-resolution image of jarosite-bearing melt inclusion with phases identified. Phase abbreviations are indicated as follows: Jar, jarosite; Tmt, titanomagnetite; Hem, hematite; Goe, goethite; Amph, Cl-rich amphibole; Po, pyrrhotite; Gl, Fe–Si rich glass; and Cpx, clinopyroxene host. The black circles with white letters indicate points for which Raman spectra were collected and correspond to spectra in Fig. 3.

(~1.8 structural formula units [sfu]), and the A-site is dominated by potassium (~0.7 sfu), therefore these are potassic-chlorohastingsites according to the nomenclature of Leake (1978) and Leake et al. (1997)

3.3. Crystal chemistry of melt inclusion jarosite

Raman spectroscopy revealed that the jarosite in Fig. 2b was actually a fine-grained mixture of jarosite, hematite,

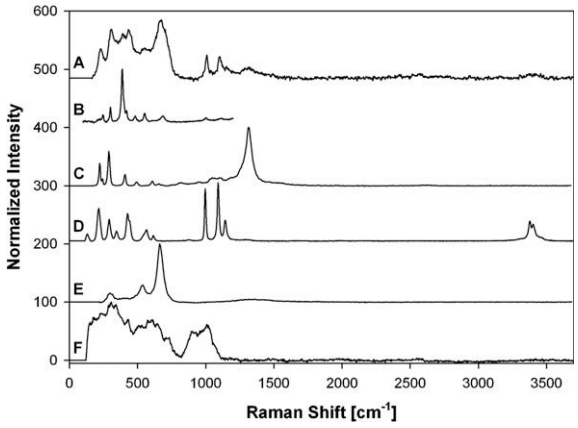

Fig. 3. Raman spectra of phases within the jarosite-bearing melt inclusion. Locations of spectra obtained from the jarosite-bearing melt inclusion are indicated in Fig. 2 by black circles with white letters corresponding to each spectrum labeled here. (A) Mixture of jarosite, hematite, and goethite collected at the edge of a titanomagnetite grain. (B) Goethite [spectrum provided by Alian Wang from Washington University, St. Louis, MO] (C) hematite [from RRuff spectral library (Downs, 2006)] (D) jarosite (E) titanomagnetite. (F) Fe–Si rich glass.

and goethite. Additionally, during EPMA analysis, a portion of the beam extended into the neighboring region of a Fe–Si-rich glass, into the titanomagnetite phase, and into a phosphate phase. This necessitated mass balance correction of the analysis (Table 1, Column 1) in order to obtain the composition of the pure jarosite (Table 1, Column 2). For this correction, first, a sufficient amount of Fe–Si-rich glass was linearly subtracted from each analysis to remove all silica. Next, titanomagnetite (composition from Table 1) was subtracted to remove all Ti. Finally, Ca was removed by apatite subtraction. Overall, the sum of overlapping phases comprised less than 10% of each analysis.

The structural formulae of the resulting compositions were then computed based on normalization to 14 anions with hematite subtraction until Fe + Al + Mg + Cr + Mn filled the M-sites in the jarosite structural formula. The amount of hematite subtraction required for each analysis ranged from about 20 to 50 wt%. Using the constraint of three M-site cations in a perfectly stoichiometric jarosite [$A_1M_3T_2O_8Z_6$], our structural formulae resulted in a T-site sum of 2.02 and an A-site sum of 1.02. The amount of H_2O was calculated such that $OH^- + Cl$ filled the Z-site. The resulting composition was then normalized to 100%.

Deconvolution of electron microprobe data for the jarosite revealed that the A-site is occupied by only K and Na (0.84 and 0.18 sfu, respectively). Because these abundances fully occupy the A-site, no hydronium (H_3O^+) component is required. The T-sites are predominantly occupied by SO_4 (1.92 sfu) with minor PO_4 substitution (0.10 sfu). The M-sites are dominated by Fe^{3+} (2.85 sfu) with minor Al (0.10 sfu), and lesser Mg, Cr, and Mn (collectively 0.05 sfu).

Although jarosite has been found previously in MIL 03346 (Herd, 2006; Vicenzi et al., 2007a), it is commonly associated with fine grained goethite and occurs within

Table 1
Electron microprobe data for phases identified within the jarosite-bearing melt inclusion.

Oxide	Jarosite*	Jarosite**	Fe–Si glass	Fe–Si glass	Ti-magnetite***	Cl-amphibole	Cl-amphibole	Pyrrhotite
SiO_2	2.32	0	45.3	45.3	0.22	35.6	35.3	–
TiO_2	0.28	0	0.19	0.07	16.6	0.24	0.24	–
Al_2O_3	0.97	0.94	8.76	3.62	3.15	10.4	9.48	–
Cr_2O_3	<0.02	0.04	<0.02	<0.02	0	<0.02	<0.02	–
Fe^T	–	–	–	–	–	–	–	58.5
$Fe_2O_3^T$	65.3	48.85	28.8	38.8	32	–	–	–
FeO^T	–	–	–	–	46.1	32.7	34.1	–
MnO	0.12	0.18	0.23	0.14	0.53	0.21	0.21	–
Co	–	–	–	–	–	–	–	0.15
Ni	–	–	–	–	–	–	–	<0.02
Cu	–	–	–	–	–	–	–	0.04
MgO	0.22	0.21	1.71	2.68	0.15	0.71	0.77	–
CaO	0.66	0	2	0.65	<0.03	10.1	9.6	–
Na_2O	0.66	1.15	0.18	0.07	0.01	0.94	0.87	–
K_2O	4.82	8.44	1.19	0.76	0.06	3.27	3.23	–
P_2O_5	1.42	1.48	3.6	0.15	<0.03	0.5	0.49	–
Cl	0.21	0.35	0.07	0.78	0	6.23	5.99	–
S^T	–	–	–	–	–	–	–	37.9
SO_3^T	18.5	32.73	0.86	0.76	0.04	–	–	–
Sb	–	–	–	–	–	–	–	<0.03
H_2O	–	5.70***	–	–	–	–	–	–
–O = Cl	0.05	0.08	0.02	0.18	0	1.41	1.35	–
Total	95.5	100	92.9	93.6	98.9	99.5	99.0	96.6

* Composition represents average of seven raw microprobe analyses of jarosite + mineral mixture.
** Composition represents the average deconvolved jarosite composition.
*** Value was calculated based on stoichiometry.
T Element measured as one oxidation state per analysis.

Table 2
Amphibole structural formulae based on 24 anions, 15 cations, and 13 cations, respectively.

Normalization to 24 anions				Normalization to 15 cations				Normalization to 13 Cations			
Si^{T}		6.14	6.16	Si^{T}		6.08	6.07	Si^{T}		6.01	5.96
Al^{T}		1.79	1.77	Al^{T}		1.85	1.86	Al^{T}		1.91	1.89
P^{T}		0.07	0.07	P^{T}		0.07	0.07	P^{T}		0.07	0.07
Fe^{3+T}		0.00	0.00	Fe^{3+T}		0.00	0.00	Fe^{3+T}		0.00	0.08
	$Total^{T}$	8.00	8.00		$Total^{T}$	8.00	8.00		$Total^{T}$	8.00	8.00
Al^{M1-3}		0.31	0.18	Al^{M1-3}		0.24	0.06	Al^{M1-3}		0.15	0.00
Ti^{M1-3}		0.03	0.03	Ti^{M1-3}		0.03	0.03	Ti^{M1-3}		0.03	0.03
Fe^{2+M1-3}		4.45	4.56	Fe^{2+M1-3}		4.08	4.02	Fe^{2+M1-3}		3.65	3.30
$Fe^{3+M1-3**}$		0.00	0.00	$Fe^{3+M1-3**}$		0.44	0.66	$Fe^{3+M1-3**}$		0.96	1.45
Mg^{M1-3}		0.18	0.20	Mg^{M1-3}		0.18	0.20	Mg^{M1-3}		0.18	0.19
Mn^{M1-3}		0.03	0.03	Mn^{M1-3}		0.03	0.03	Mn^{M1-3}		0.03	0.03
	$Total^{M1-3}$	5.00	5.00		$Total^{M1-3}$	5.00	5.00		$Total^{M1-3}$	5.00	5.00
Fe^{M4}		0.26	0.42	Fe^{M4}		0.15	0.23	Fe^{M4}		0.00	0.00
Ca^{M4}		1.74	1.58	Ca^{M4}		1.85	1.77	Ca^{M4}		1.83	1.74
Na^{M4}		0.00	0.00	Na^{M4}		0.00	0.00	Na^{M4}		0.17	0.26
	$Total^{M4}$	2.00	2.00		$Total^{M4}$	2.00	2.00		$Total^{M4}$	2.00	2.00
Ca^{A}		0.13	0.22	Ca^{A}		0.00	0.00	Ca^{A}		0.00	0.00
Na^{A}		0.31	0.29	Na^{A}		0.31	0.29	Na^{A}		0.14	0.02
K^{A}		0.72	0.72	K^{A}		0.71	0.71	K^{A}		0.71	0.70
	$Total^{A}$	1.16	1.23		$Total^{A}$	1.02	1.00		$Total^{A}$	0.85	0.72
$Cl^{O(3)}$		1.82	1.77	$Cl^{O(3)}$		1.80	1.75	$Cl^{O(3)}$		1.78	1.72
$OH^{O(3)*}$		0.18	0.23	$OH^{O(3)*}$		0.20	0.25	$OH^{O(3)*}$		0.22	0.28
	$Total^{O(3)}$	2.00	2.00		$Total^{O(3)}$	2.00	2.00		$Total^{O(3)}$	2.00	2.00

Amphibole formula: $(K_{0.71}Na_{0.30})(Ca_{1.81}Fe^{2+}{}_{0.19})(Fe2+_{4.05}Fe^{3+}{}_{0.55}Mn_{0.03}Mg_{0.19}Al_{0.15}Ti_{0.03})[Si_{6.08}Al_{1.85}P_{0.07}O_{22}](Cl_{1.78}(OH)_{0.22})$.
* Based on stoichiometry assuming OH + Cl = full O(3) site (presence of OH was verified by Raman spectroscopy).
** Based on charge balance.

small veins and fractures (Herd, 2006; Vicenzi et al., 2007a). Based on D/H isotopic ratios and textural evidence, Vicenzi et al. (2007b) concluded that the vein jarosite is likely martian in origin and associated with aqueous alteration on the martian surface. The presence of goethite rather than hematite in the veins suggests jarosite formation in the presence of low-temperature (<100 °C) acidic oxidizing aqueous fluids (Cornell and Schwertmann, 2003) in a process similar to that invoked for the jarosite found at Meridiani Planum (Squyres et al., 2004, 2006). This vein jarosite is distinct from the melt inclusion jarosite identified in our study, which is confined to the melt inclusion and coexists with hematite and goethite.

4. DISCUSSION

4.1. High-temperature hydrothermal history of MIL 03346

Chlorine-rich potassic-hastingsite typically forms from hydrothermal or metasomatic fluids below the solidus temperature of the silicate melt (Vanko, 1986; Leger et al., 1996; Sato et al., 1997; i.e., Kullerud and Erambert, 1999; Polovina et al., 2004), although pinpointing the maximum thermal stability has been hindered by a paucity of experimental data. In fact, Mazdab (2003) reported that potassic-chlorohastingsite (>2 wt% Cl) is typical of alkali–halide metasomatism associated with various types of ore-mineralization. Therefore the potassic-chlorohastingsite in the melt inclusion of MIL 03346 likely formed from a chlorine-rich fluid. This fluid could have either formed from the trapped melt during crystallization once fluid-saturation was attained (endogenous fluid), or from elsewhere in the magma plumbing system, becoming trapped along with surrounding melt by the growing pyroxene crystals (exogenous fluid). Importantly, the high chlorine/hydroxyl ratio of the potassic-chlorohastingsite (⩾9:1) indicates that chlorine activity was very high in the fluid, and the possibility of the fluid having been an alkali–halide melt cannot be excluded (Mazdab, 2003).

The presence of pyrrhotite and titano-magnetite in the melt inclusion indicates that the melt and/or fluid had elevated concentrations of iron, sulfur and titanium at the time of entrapment. Given the large collective area occupied by the potassic-chlorohastingsite, pyrrhotite, and titano-magnetite in Fig. 2b, it seems likely that the oxide and sulfide were included with melt at the time of entrapment (hence the melt was saturated with respect to these phases). Alternatively, an exogenous fluid was trapped with melt in the inclusion, and the fluid was responsible for precipitating the potassic-chlorohastingsite, titanomagnetite and pyrrhotite. Regardless of which is the case, the hydrothermal fluid was elevated in the volatiles Cl and S.

Water-bearing fluids high in NaCl- and/or KCl-components are likely to undergo phase separation (into L + V) even at elevated pressure and temperature (⩽1500 bars and 800 °C (Liebscher, 2007)). Moreover, the presence of additional components in the fluid (e.g., S-species) would widen the immiscible vapor–liquid region to even higher temperatures and pressures (Webster and Mandeville, 2007). The vapor phase will be enriched in HCl and H_2S (and potentially HF, Si, B, and Cu) while the aqueous liquid would become enriched in alkalis, alkaline earths,

and Fe-chlorides and sulfates (Hedenquist and Lowenstern, 1994; Shmulovich et al., 1995; Bischoff et al., 1996; Shmulovich et al., 2002; Baker et al., 2004). If this process were occurring in the melt interstitial to the cumulus clinopyroxene grains, the vapor phase could readily separate and leave the system. With potentially significant partitioning of H_2S into the vapor relative to SO_2 (Ohmoto and Rye, 1979; Delmelle et al., 2000; Webster and Mandeville, 2007), this vapor loss could increase the oxidation state of the magma as a whole, causing it to become increasingly oxidized as cooling proceeds. This may have been the mechanism behind the late oxidation of the cumulus pyroxene rims and the mesostasis.

Within a melt inclusion, however, both aqueous liquid and vapor could coexist. The over-pressure induced by the phase separation may have been responsible for the extensive melt inclusion rupture observed. Any melt inclusions that remained sealed were, in part, protected from the pervasive magmatic oxidation outside of the cumulus grains due to the redox capacity of the hosting cumulus pyroxene grains, shown to be at an oxygen fugacity of IW + 2.2 (Domeneghetti et al., 2006). However, diffusive hydrogen loss from the sealed melt inclusions would have been driven by the coupling of two processes: (1) the over-pressure induced by phase separation within the sealed melt inclusions and (2) the difference in chemical potential of hydrogen between the sealed melt inclusions and the mesostasis that occurred as a result of lost H-species during phase separation of the fluid in the mesostasis. These processes would work to oxidize the melt inclusion as a function of the degree of molecular dissociation of water and of the rate of H-diffusion through the clinopyroxene host.

Given the calculated low ferric iron content of the potassic-chlorohastingsite, the fluid was probably not very oxidized at the time of amphibole precipitation (i.e., King et al., 2000). However, this could be a result of the redox capacity of the hosting cumulus pyroxene grains. Therefore, even if vapor loss were responsible for the extensive late magmatic oxidation observed in the mesostasis and cumulus pyroxene rims, we cannot determine whether or not the potassic-chlorohastingsite precipitated before or after L + V separation occurred.

4.2. Low-temperature hydrothermal history of MIL 03346

The absence of H_3O from the A-site of the melt inclusion jarosite is consistent with formation under hydrothermal conditions (Brophy and Sheridan, 1965; Stoffregen, 1993) since H_3O-subsitution in jarosite is ubiquitous at low-temperatures and pressures, but it does not occur above 100 °C. The partitioning of sulfate into the liquid phase during L + V separation in the melt inclusion suggests that the aqueous liquid likely played the dominant role in jarosite formation. Because jarosite precipitation requires the presence of oxidized liquids, this oxidation must have occurred after precipitation of the potassic-chlorohastingsite. Existing thermochemical data can be used to constrain the hydrothermal redox conditions of the liquid during jarosite formation. Fig. 4 shows a calculated stability diagram for pure K-jarosite, hematite, and pyrrhotite at

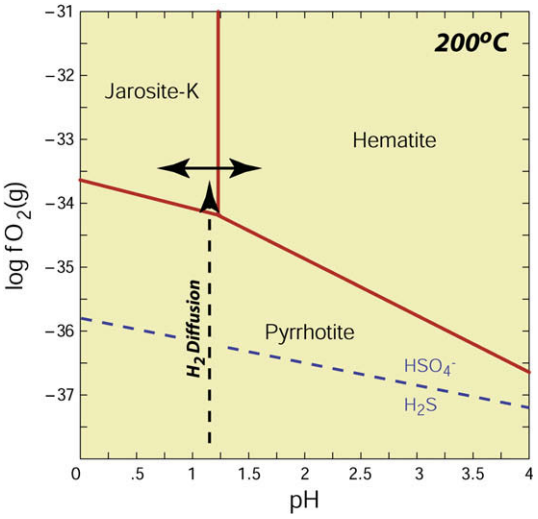

Fig. 4. Computed jarosite stability diagram for 200 °C and 100 bars (after Stoffregen (1993)). Thermodynamic data for endmember K–jarosite were obtained from Stoffregen et al. (2000). Data for pyrrhotite and hematite were taken from Robie and Hemingway (1995). The diagram was constructed with log $a_{SO4} = -0.5$ and log $a_K = -0.5$. The dashed black line indicates the probable reaction pathway of H_2 diffusion in pH-logfO_2 space. The HSO_4^-–H_2S equilibrium curve under these conditions is indicated in blue. The possible range in pH that jarosite–hematite co-precipitation is known to occur is indicated by the two black arrows connected by a solid black line.

200 °C (assuming that oxidation was rapid enough to prevent the formation of secondary sulfide). At this temperature, a log fO_2 of at least −34 must be attained before jarosite begins to precipitate. Importantly, although an external oxidation event may have occurred as implied by the oxidized mesostasis and cumulus pyroxene rims, the oxygen fugacity required for jarosite precipitation within the melt inclusion would be attained by diffusive hydrogen loss coupled with the decreasing temperature of the liquid (Fig. 4). Although a precise jarosite formation temperature cannot be determined, this lower redox boundary may be plotted as a function of temperature in order to obtain a range of possible conditions that would allow jarosite precipitation (Fig. 5).

The composition of the jarosite provides important constraints on the chemical nature of this liquid phase. The jarosite composition is largely potassic (K^+ fills 83% of the A-site) suggesting that the K^+/Na^+ activity ratio of the aqueous liquid at this stage was too high to incorporate abundant Na into the jarosite structure (Alpers et al., 1989; Stoffregen et al., 2000). Importantly, the potassic nature of the aqueous phase is consistent with the potassic nature of both of the amorphous phases found in the melt inclusion and the potassic-chlorohastingsite. This further suggests that the melt inclusion jarosite formed from a liquid that had chemical characteristics similar to the high-temperature fluid responsible for precipitating the potassic-chlorohastingsite.

The association of jarosite with other minerals can also provide insights into reactions between the aqueous liquid

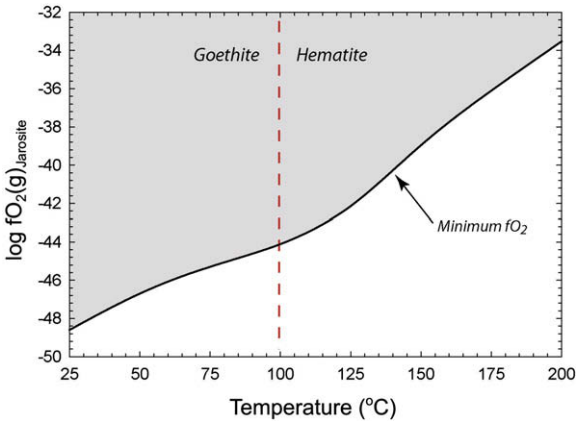

Fig. 5. Calculated minimum oxygen fugacities log fO_2(g) required for jarosite formation as a function of temperature. The dashed line indicates the temperature of the goethite–hematite transition.

and the melt inclusion minerals below the temperature of initial saturation with jarosite. Both goethite and hematite are found with jarosite in the melt inclusion and this association aids in constraining the pH of the fluid (Alpers et al., 1989). Fig. 4 shows that the coexistence of jarosite and hematite would require the pH of the fluid to remain close to the jarosite/hematite boundary (approximately 1.2 at 200 °C). The low pH required for jarosite precipitation was likely obtained by oxidation of the pyrrhotite as it interacted with the cooling, increasingly oxidizing liquid.

The presence of goethite in the sample indicates that the parental liquid cooled to a temperature below 100 °C (the goethite–hematite transition) and remained at this temperature long enough to precipitate goethite (Fig. 6). At

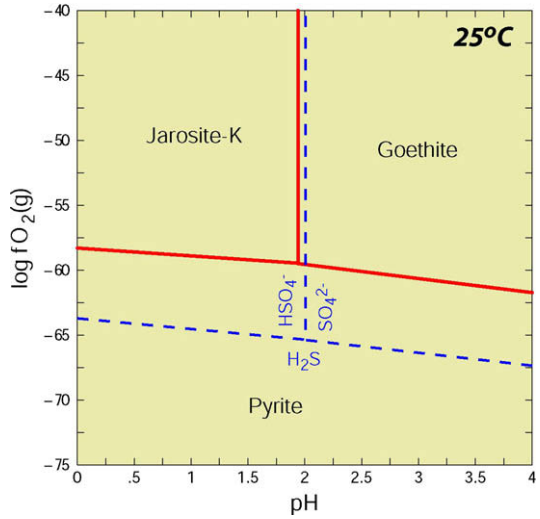

Fig. 6. Computed jarosite stability diagram for 25 °C and 1 bars (after Stoffregen (1993)). Thermodynamic data for endmember K–jarosite were obtained from Stoffregen et al. (2000). Data for pyrite and goethite were taken from Robie and Hemingway (1995). The diagram was constructed with log $a_{SO4} = -0.5$ and log $a_K = -0.5$. The HSO_4^-–H_2S–SO_4^{2-} equilibrium curves under these conditions are indicated in blue.

25 °C, goethite is more likely to be initially formed (Cornell and Schwertmann, 2003), requiring a pH of approximately 1.9 to result in goethite–jarosite co-precipitation (Fig. 6). The jarosite within the melt inclusion then, is likely to have precipitated continuously over a range of temperatures.

Complete solid solution exists between the iron and aluminum endmembers of jarosite–alunite compositions (Stoffregen et al., 2000). The melt inclusion jarosite analyzed in this study contains significant Fe and only a small proportion of Al (0.10 sfu) in the M-site in spite of the presence of significant available Al (as evidenced by the presence of the aluminous Fe–Si glass). This suggests that the parental liquids were dominated by Fe and that the pH of the parental aqueous phase was too low to facilitate hydrolysis of Al. Hydrolysis of aluminum would result in either significant Al incorporation into the jarosite structure or, at high Al and SO_4 activity, the precipitation of an alunite phase.

4.3. Implications for wide-scale martian alteration environments

The discovery of jarosite, hematite, and goethite in a melt inclusion within MIL 03346 provides the first direct evidence that martian magmatic fluids have evolved to low-temperature aqueous phases responsible for precipitating alteration assemblages that have been observed on the surface of Mars. The strong textural evidence for the formation of the melt inclusion jarosite by oxidation of a primary magmatic sulfide represents the first documented evidence for such a jarosite formation pathway on Mars [although it has been previously suggested (Burns, 1986, 1987, 1988; Burns and Fisher, 1990a,b)]. Jarosite formation by sulfide oxidation is not limited to high-temperatures or pressures and would likely occur wherever liquid water interacts with sulfides in martian rocks. On Earth, in mine waste environments, sulfide mineral oxidation is a common pathway for the formation of jarosite, goethite and hematite (Alpers et al., 1989). Such terrestrial environments also commonly host a rich and diverse community of microorganisms which thrive in the acidic, oxidizing fluids produced during the process (Alpers et al., 1989), although the ability to withstand acidity and salinity stress are the result of evolutionary mechanisms possibly requiring prolonged geological timescales. In addition, coupling of these environments with potentially high chlorine activities and, by inference, low water activity, may limit the chances that these environments were, in fact, cradles for life at the martian subsurface (Tosca et al., 2008b).

4.4. Implications for ore-formation on Mars

MIL 03346 is the second martian meteorite to show definitive evidence for interaction with Cl-rich hydrothermal fluids [Chassigny also exhibits such evidence (McCubbin and Nekvasil, 2008)]. Hydrothermal alteration of martian rocks by magmatically derived Cl-rich fluids may have implications for ore-deposition on Mars. Ore bodies on Earth are largely correlated to chlorine "hot-spots" because many transition metals, including the platinum group elements (PGE), partition strongly into chlorine-rich fluids

at elevated temperature (i.e., Li and Naldrett, 1993; Kislov et al., 1997; Willmore et al., 2000; Mungall and Brenan, 2003). These deposits are often accompanied by mineral assemblages consisting of sulfides and Cl-rich phases such as chlorapatite and chlor-amphiboles (i.e., Boudreau and McCallum, 1989, 1992; Boudreau, 1993; Meurer and Boudreau, 1996; Webster, 1997; Willmore et al., 2000; Mazdab, 2003; Mungall and Brenan, 2003).

Apatite from all martian meteorites have been identified as predominantly Cl-rich (Greenwood, 2005), suggesting the possibility that chlorine-rich hydrothermal fluids may be widespread in martian igneous systems. However, if all the martian meteorites came from one geographically limited area, we could be seeing a limited slice of what martian magmatism has to offer. Because we lack sufficiently detailed geologic context for martian meteorites, and we have no way of assessing whether these rocks are representative or recording rare magmatic processes, sample return is a necessary next step in furthering our understanding of martian magmatism.

5. SUMMARY

The jarosite-bearing melt inclusion in MIL 03346 has recorded a magmatic-hydrothermal history in its hosted phases (titanomagnetite, pyrrhotite, Cl-rich amphibole, and jarosite). This history begins at entrapment of silicate melt (±previously crystallized pyrrhotite and titanomagnetite and ±fluid?) with an elevated volatile load that exsolved a fluid phase once sufficient crystallization occurred for fluid-saturation. This fluid, rich in chlorine, reacted with surrounding silicate material to produce the potassic-chlorohastingsite. As cooling proceeded, the fluid separated into liquid and vapor phases, marked by increasing pressure within the sealed melt inclusion, causing many of the inclusions to rupture. Within the inclusions that remained sealed, the liquid phase eventually became more oxidized (as a function of temperature and H-diffusion) and, in the case of the jarosite-bearing melt inclusion, reacted with the trapped pyrrhotite grain. Sulfide oxidation resulted in SO_4^{2-} formation and concomitant acid production, setting the stage for jarosite formation, beginning possibly as high as ~200 °C. As the fluid cooled below 200 °C, jarosite continued to precipitate with hematite and/or goethite until equilibrium was established or reactions became kinetically unfavorable.

ACKNOWLEDGMENTS

We thank the Antarctic Meteorite Working Group and the Meteorite curatorial staff at the Lyndon B. Johnson Space Center in Houston, TX for approving our request and allocating a thin section of MIL 03346 (#114). We would also like to thank Christopher Herd, Harry McSween, and one anonymous reviewer for helpful and insightful reviews of the manuscript. We are grateful to Alan Brandon for the editorial handling of the paper. Financial support for this work was provided by NASA grant NNX08AN14G from the Mars Fundamental Research Program awarded to Hanna Nekvasil and Andrew Steele acknowledges financial support from the NASA SERLIDA program. Francis McCubbin is grateful for a Graduate Assistance in Areas of National Need (GAANN) Fellowship. Nicholas Tosca was supported by an Origins Postdoctoral Fellowship. Alexander Smirnov acknowledges fellowship support from the Carnegie Institution of Washington, Geophysical Laboratory and NASA Astrobiology Institute during this study.

REFERENCES

Alpers C. N., Nordstrom D. K. and Ball J. W. (1989) Solubility of jarosite solid solutions precipitated from acid mine waters, iron Mountain, California, USA. *Sci. Geol. Bull.* **42**, 281–298.

Aoudjehane H. C., Jambon A. and Boudouma O. (2006) A cathodoluminescence study of cristobalite and K-feldspar in the nakhlite Mil 03346. *Meteorit. Planet. Sci.* **41**, A37.

Baker T., Van Achterberg E., Ryan C. G. and Lang J. R. (2004) Composition and evolution of ore fluids in a magmatic-hydrothermal skarn deposits. *Geology* **32**, 117–120.

Bischoff J. L., Rosenbauer R. J. and Fournier R. O. (1996) The generation of HCl in the system CaCl2–H2O: vapor-liquid relations from 380–500 °C. *Geochim. Cosmochim. Acta* **60**, 7–16.

Boudreau A. E. (1993) Chlorine as an exploration guide for the platinum-group elements in layered intrusions. *J. Geochem. Explor.* **48**, 21–37.

Boudreau A. E. and McCallum I. S. (1989) Investigations of the Stillwater complex: part V. Apatites as indicators of evolving fluid composition. *Contrib. Mineral. Petrol.* **102**, 138–153.

Boudreau A. E. and McCallum I. S. (1992) Infiltration metasomatism in layered intrusions–an example from the Stillwater complex, Montana. *J. Volcanol. Geoth. Res.* **52**, 171–183.

Bridges J. C., Catling D. C., Saxton J. M., Swindle T. D., Lyon I. C. and Grady M. M. (2001) Alteration assemblages in martian meteorites: implications for near-surface processes. *Space Sci. Rev.* **96**, 365–392.

Brophy G. P. and Sheridan M. F. (1965) Sulfate studies IV. Jarosite–natrojarosite–hydronium jarosite solid solution series. *Am. Mineral.* **50**, 1595.

Burns R. G. (1986) Terrestrial analogs of the surface rocks of Mars. *Nature* **320**, 55–56.

Burns R. G. (1987) Ferric sulfates on Mars. *J. Geophys. Res. Solid Earth Planet.* **92**, E570–E574.

Burns, R. G., 1988. Gossans on mars. In *Proceedings of the 18th Lunar and Planetary Science Conference*. LPI, Houston, TX.

Burns R. G. and Fisher D. S. (1990a) Evolution of sulfide mineralization on Mars. *J. Geophys. Res. Solid Earth Planet.* **95**, 14169–14173.

Burns R. G. and Fisher D. S. (1990b) Iron–sulfur mineralogy of Mars - magmatic evolution and chemical-weathering products. *J. Geophys. Res. Planet.* **95**, 14415–14421.

Cornell R. M. and Schwertmann U. (2003) The Iron Oxides: Structure, Properties, Reactions, Occurrences and Uses. Wiley, Weinheim.

Day J. M. D., Taylor L. A., Floss C. and McSween H. Y. (2006) Petrology and chemistry of Mil 03346 and its significance in understanding the petrogenesis of nakhlites on Mars. *Meteorit. Planet. Sci.* **41**, 581–606.

Delmelle P., Bernard A., Kusakabe M., Fischer T. P. and Takano B. (2000) Geochemistry of the magmatic-hydrothermal system of Kawah Ijen volcano, East Java, Indonesia. *j. Volcanol. Geoth. Res.* **97**, 31–53.

Domeneghetti, M. C., Fioretti, A. M., Camara, F., Carraro, A., McCammon, C. and Tazzoli, V., 2007. Constraints on the thermal history of martian meteorites ALH 84001 and Mil 03346 by single crystal XRD, electron microprobe and

Mössbauer analyses of ortho- and clinopyroxene. In *7th International Conference on Mars*, Pasadena, CA.

Domeneghetti, M. C., Fioretti, A. M., Camara, F., Molin, G. and McCammon, C., 2006. Constraints on the thermal history and oxidation state of Mil03346 martian meteorite: single-crystal XRD, electron microprobe and Mössbauer analyses of clinopyroxene. In *Proceedings of the 37th Lunar and Planetary science conference*, Houston, TX.

Downs, R. T., 2006. The rruff project: an integrated study of the chemistry, crystallography, Raman and infrared spectroscopy of minerals. *19th General Meeting of the International Mineralogical Association Kobe*, Japan.

Dyar M. D., Treiman A. H., Pieters C. M., Hiroi T., Lane M. D. and O'Connor V. (2005) Mil03346, the most oxidized martian meteorite: a first look at spectroscopy, petrography, and mineral chemistry. *J. Geophys. Res. Planet.* **110**.

Glotch T. D., Morris R. V., Christensen P. R. and Sharp T. G. (2004) Effect of precursor mineralogy on the thermal infrared emission spectra of hematite: application to martian hematite mineralization. *J. Geophys. Res. Planet.* **109**.

Glotch T. D. and Rogers A. D. (2007) Evidence for aqueous deposition of hematite- and sulfate-rich light-toned layered deposits in Aureum and Iani Chaos, Mars. *J. Geophys. Res. Planet.* **112**, 2–3.

Greenwood J. P. (2005) Chlorine-rich apatites in SNC's: evidence for magma-brine interactions on Mars? *Meteorit. Planet. Sci.* **40**, A60.

Hedenquist J. W. and Lowenstern J. B. (1994) The role of magmas in the formation of hydrothermal ore-deposits. *Nature* **370**, 519–527.

Herd C. D. K. (2006) An occurrence of jarosite in Mil 03346: implications for conditions of martian aqueous alteration. *Meteorit. Planet. Sci.* **41**, A74.

Hurowitz J. A. and McLennan S. M. (2007) A similar to 3.5 Ga record of water-limited, acidic weathering conditions on Mars. *Earth Planet. Sci. Lett.* **260**, 432–443.

Imae N. and Ikeda Y. (2007) Petrology of the Miller Range 03346 nakhlite in comparison with the Yamato-000593 nakhlite. *Meteorit. Planet. Sci.* **42**, 171–184.

King P. L., Hervig R. L., Holloway J. R., Delaney J. S. and Dyar M. D. (2000) Partitioning of Fe^{3+}/Fe-total between amphibole and basanitic melt as a function of oxygen fugacity. *Earth Planet. Sci. Lett.* **178**, 97–112.

King P. L. and McSween H. Y. (2005) Effects of H_2O, pH, and oxidation state on the stability of Fe minerals on Mars. *J. Geophys. Res. Planet.* **110**.

Kislov E. V., Konnikov E. G., Orsoev D. A., Pushkarev E. V. and Voronina L. K. (1997) Chlorine in the genesis of the low-sulfide PGE mineralization in the Ioko-dovyrenskii Layered Massif. *Geokhimiya*, 521–528.

Kullerud K. and Erambert M. (1999) Cl-scapolite, Cl-amphibole, and plagioclase equilibria in ductile shear zones at Nusfjord, Lofoten, Norway: implications for fluid compositional evolution during fluid-mineral interaction in the deep crust. *Geochim. Cosmochim. Acta* **63**, 3829–3844.

Leake B. E. (1978) Nomenclature of amphiboles. *Am. Mineral.* **63**, 1023–1052.

Leake B. E., Woolley A. R., Arps C. E. S., Birch W. D., Gilbert M. C., Grice J. D., Hawthorne F. C., Kato A., Kisch H. J., Krivovichev V. G., Linthout K., Laird J., Mandarino J. A., Maresch W. V., Nickel E. H., Rock N. M. S., Schumacher J. C., Smith D. C., Stephenson N. C. N., Ungaretti L., Whittaker E. J. W. and Guo Y. Z. (1997) Nomenclature of amphiboles: report of the subcommittee on amphiboles of the international mineralogical association, commission on new minerals and mineral names. *Can. Mineral.* **35**, 219–246.

Leger A., Rebbert C. and Webster J. (1996) Cl-rich biotite and amphibole from black rock forest, Cornwall, New York. *Am. Mineral.* **81**, 495–504.

Li C. and Naldrett A. J. (1993) High chlorine alteration minerals and calcium-rich brines in fluid inclusions from the Strathcona deep copper zone, Sudbury, Ontario. *Econ. Geol. Bull. Soc.* **88**, 1780–1796.

Liebscher A. (2007). *Experimental Studies in Model Fluid Systems*. .

Madden M. E. E., Bodnar R. J. and Rimstidt J. D. (2004) Jarosite as an indicator of water-limited chemical weathering on Mars. *Nature* **431**, 821–823.

Mazdab F. K. (2003) The diversity and occurrence of potassium-dominant amphiboles. *Can. Mineral.* **41**, 1329–1344.

McCormick K. A. and McDonald A. M. (1999) Chlorine-bearing amphiboles from the Fraser Mine, Sudbury, Ontario, Canada: description and crystal chemistry. *Can. Mineral.* **37**, 1385–1403.

McCubbin F. M. and Nekvasil H. (2008) Maskelynite-hosted apatite in the Chassigny meteorite: insights into late-stage magmatic volatile evolution in martian magmas. *Am. Mineral.* **93**, 676–684.

McLennan S. M., Bell J. F., Calvin W. M., Christensen P. R., Clark B. C., de Souza P. A., Farmer J., Farrand W. H., Fike D. A., Gellert R., Ghosh A., Glotch T. D., Grotzinger J. P., Hahn B., Herkenhoff K. E., Hurowitz J. A., Johnson J. R., Johnson S. S., Jolliff B., Klingelhofer G., Knoll A. H., Learner Z., Malin M. C., McSween H. Y., Pocock J., Ruff S. W., Soderblom L. A., Squyres S. W., Tosca N. J., Watters W. A., Wyatt M. B. and Yen A. (2005) Provenance and diagenesis of the evaporite-bearing burns formation, Meridiani Planum, Mars. *Earth and Planet. Sci. Lett.* **240**, 95–121.

Meurer W. P. and Boudreau A. E. (1996) An evaluation of models of apatite compositional variability using apatite from the middle banded series of the Stillwater complex, Montana. *Contrib. Mineral. Petrol.* **125**, 225–236.

Mungall J. E. and Brenan J. M. (2003) Experimental evidence for the chalcophile behavior of the halogens. *Can. Mineral.* **41**, 207–220.

Navrotsky A., Forray F. L. and Drouet C. (2005) Jarosite stability on Mars. *Icarus* **176**, 250–253.

Ohmoto H. and Rye R. O. (1979) Isotopes of sulfur and carbon. In *Geochemistry of Hydrothermal Ore Deposits* (ed. H. L. Barnes). Wiley, New York.

Papike J. J., Karner J. M. and Shearer C. K. (2006) Comparative planetary mineralogy: implications of martian and terrestrial jarosite. A crystal chemical perspective. *Geochim. Cosmochim. Acta* **70**, 1309–1321.

Polovina J. S., Hudson D. M. and Jones R. E. (2004) Petrographic and geochemical characteristics of postmagmatic hydrothermal alteration and mineralization in the j-m reef, Stillwater complex, Montana. *Can. Mineral.* **42**, 261–277.

Righter K., Yang H., Costin G. and Downs R. T. (2008) Oxygen fugacity in the martian mantle controlled by carbon: new constraints from the nakhlite Mil 03346. *Meteorit. Planet. Sci.* **43**, 1709–1723.

Robie R. A. and Hemingway D. S. (1995) Thermodynamic properties of minerals and related substances at 298.15 K and 1 bar (105 pascals) pressure and at higher temperatures. *USGS Bull.* **2131**, 461.

Sato H., Yamaguchi Y. and Makino K. (1997) Cl incorporation into successively zoned amphiboles from the Ramnes Cauldron, Norway. *Am. Mineral.* **82**, 316–324.

Sautter V., Jambon A. and Boudouma O. (2006) Cl-amphibole in the nakhlite Mil 03346: evidence for sediment contamination in a martian meteorite. *Earth and Planet. Sci. Lett.* **252**, 45–55.

Shmulovich K., Heinrich W., Moller P. and Dulski P. (2002) Experimental determination of REE fractionation between

liquid and vapor in the systems NaCl–H_2O and $CaCl_2$–H_2O up to 450 °C. *Contrib, Mineral, Petrol,* **144**, 257–273.

Shmulovich K. I., Tkachenko S. I. and Plyasunova N. V. (1995) Phase equilibria in fluid systems at high pressures and temperatures. In *Fluids in the Crust: Equilibrium and Transport Properties* (eds. K. I. Shmulovich, B. W. D. Yardley and G. A. Gonchar). Chapman and Hall, London.

Squyres S. W., Grotzinger J. P., Arvidson R. E., Bell, III, J. F., Christensen P. R., Clark B. C., Crisp J. A., Farrand W., Herkenhoff K. E., Johnson J. R., Klingelhöfer G., Knoll A. H., McLennan S. M., McSween H. Y., Morris R. V., Rice J. W., Rieder R. and Soderblom L. A. (2004) In-situ evidence for an ancient aqueous environment at Meridiani Planum, Mars. *Science* **306**, 1709.

Squyres S. W., Knoll A. H., Arvidson R. E., Clark B. C., Grotzinger J. P., Jolliff B. L., McLennan S. M., Tosca N. J., Bell J. F., Calvin W. M., Farrand W. H., Glotch T. D., Golombek M. P., Herkenhoff K. E., Johnson J. R., Klingelhoefer G., McSween H. Y. and Yen A. S. (2006) Two years at Meridiani Planum: results from the opportunity rover. *Science* **313**, 1403–1407.

Steele A., Fries M. D., Amundsen H. E. F., Mysen B. O., Fogel M. L., Schweizer M. and Boctor N. Z. (2007) Comprehensive imaging and Raman spectroscopy of carbonate globules from martian meteorite ALH 84001 and a terrestrial analogue from Svalbard. *Meteorit. Planet. Sci.* **42**, 1549–1566.

Stoffregen R. E. (1993) Stability relations of jarosite and natrojarosite at 150–250 °C. *Geochim. Cosmochim. Acta* **57**, 2417.

Stoffregen R. E., Alpers C. N. and Jambor J. L. (2000) Alunite-jarosite crystallography, thermodynamics and geochronology. In *Sulfate Minerals: Crystallography, Geochemistry and Environmental Significance* (eds. C. N. Alpers, J. L. Jambor and D. K. Nordstrom). Mineralogical Society of America, Washington, DC.

Tosca N. J., McLennan S. M., Dyar M. D., Sklute E. C. and Michel F. M. (2008a) Fe oxidation processes at Meridiani Planum and implications for secondary Fe mineralogy on Mars. *J. Geophys. Res. Planet.* **113**.

Tosca N. J., McLennan S. M., Clark B. C., Grotzinger J. P., Hurowitz J. A., Knoll A. H., Schroder C. and Squyres S. W. (2005) Geochemical modeling of evaporation processes on Mars: insight from the sedimentary record at Meridiani Planum. *Earth Planet. Sci. Lett.* **240**, 122–148.

Tosca N. J., Knoll A. H. and McLennan S. M. (2008b) Water activity and the challenge for life on early Mars. *Science* **320**, 1204–1207.

Treiman A. H. (2005) The nakhlite meteorites: augite-rich igneous rocks from Mars. *Chemie Der Erde-Geochem.* **65**, 203–270.

Vanko D. A. (1986) High-chlorine amphiboles from oceanic rocks – product of highly-saline hydrothermal fluids. *Am. Mineral.* **71**, 51–59.

Veksler I. V. (2006) Crystallized melt inclusions in gabbroic rocks, melt inclusions in plutonic rocks (ed. J. D. Webster). Mineralogical Association of Canada, Montreal.

Vicenzi, E. P., Fries, M., Fahey, A., Rost, D., Greenwood, J. P. and Steele, A., 2007a. Detailed elemental, mineralgical, and isotopic examination of jarosite in martian meteorite Mil 03346. In *Poceedings of the Lunar and Planetary Science Conference XXXVIII*, Houston, TX.

Vicenzi E. P., Fries M., Fahey A., Rost D., Greenwood J. P. and Steele A. (2007b) Evidence for young jarosite precipitation on Mars. *Meteorit. Planet. Sci.* **42**, A157.

Webster J. D. (1997) Exsolution of magmatic volatile phases from Cl-enriched mineralizing granitic magmas and implications for ore metal transport. *Geochim. Cosmochim. Acta* **61**, 1017–1029.

Webster J. D. and Mandeville C. W. (2007) Fluid immiscibility in volcanic environments. *Fluid-fluid interactions* **65**, 313–362.

Willmore C. C., Boudreau A. E. and Kruger F. J. (2000) The halogen geochemistry of the Bushveld complex, Republic of South Africa: implications for chalcophile element distribution in the lower and critical zones. *J. Petrol.* **41**, 1517–1539.

Associate editor: Alan D. Brandon